

## PREPRINT STATEMENT

---

This manuscript has been submitted for publication in *Radiation Measurements*. Please note that this study has not yet undergone peer-review or been accepted for publication. Subsequent versions of this manuscript may have slightly different content. If accepted, the final version of this manuscript will be available via the '*Peer-reviewed Publication DOI*' link above this window.

---

# Developing an internally consistent methodology for K-feldspar MAAD TL thermochronology

N.D. Brown<sup>a,b,c,\*</sup>, E.J. Rhodes<sup>b,d</sup>

<sup>a</sup>*Department of Earth and Planetary Science, University of California, Berkeley, CA, USA*

<sup>b</sup>*Department of Earth, Planetary, and Space Sciences, University of California, Los Angeles, CA, USA*

<sup>c</sup>*Department of Earth and Environmental Sciences, University of Texas, Arlington, TX, USA*

<sup>d</sup>*Department of Geography, University of Sheffield, UK*

---

## Abstract

Luminescence thermochronology and thermometry can quantify recent changes in rock exhumation rates and rock surface temperatures, but these methods require accurate determination of several kinetic parameters. For K-feldspar thermoluminescence (TL) glow curves, which comprise overlapping signals of different thermal stability, it is challenging to develop measurements that capture these parameter values. Here, we present multiple-aliquot additive-dose (MAAD) TL dose response and fading measurements from bedrock-extracted K-feldspars. These measurements are compared with Monte Carlo simulations to identify best-fit values for recombination center density ( $\rho$ ) and activation energy ( $\Delta E$ ). This is done for each dataset separately, and then by combining dose-response and fading misfits to yield more precise  $\rho$  and  $\Delta E$  values consistent with both experiments. Finally, these values are used to estimate the characteristic dose ( $D_0$ ) of samples. This approach produces kinetic parameter values consistent with comparable studies and results in expected fractional saturation differences between samples.

*Keywords:* Feldspar thermoluminescence, low-temperature thermochronology, kinetic parameters

---

\*Corresponding author

*Email address:* `nathan.brown@uta.edu` (N.D. Brown)

## 1. Introduction

Recent work has shown that luminescence signals can be used to study the time-temperature history of quartz or feldspar grains within bedrock. Applications include estimations of near-surface exhumation (Herman et al., 2010; King et al., 2016b; Biswas et al., 2018), borehole temperatures (Guralnik et al., 2015; Brown et al., 2017), and even past rock temperatures at Earth’s surface (Biswas et al., 2020). While luminescence thermochronology and thermochronometry provide useful records of recent erosion and temperature changes, these methods depend upon which kinetic model is assumed and how the relevant parameters are determined (cf. Li and Li, 2012; King et al., 2016b; Brown et al., 2017).

In this study, we demonstrate how a multiple-aliquot additive-dose (MAAD) thermoluminescence (TL) protocol can yield internally consistent estimates of recombination center density,  $\rho$  ( $\text{m}^{-3}$ ), and activation energy,  $\Delta E$  (eV), in addition to the other kinetic parameters needed to determine fractional saturation as a function of measurement temperature,  $\frac{n}{N}(T)$  (Fig. 1). In MAAD protocols, naturally irradiated aliquots are given an additional laboratory dose before the TL signals are measured. By contrast, the widely used single-aliquot regenerative-dose (SAR) protocol produces a dose-response curve and  $D_e$  estimate from individual aliquots which, after the natural measurement, are repeatedly irradiated and measured, each time filling the traps before emptying them during the measurement (Wintle and Murray, 2006). One advantage of a SAR protocol is that each disc yields an independent  $D_e$  estimate, which can be measured to optimal resolution by incorporating many dose points. This ensures that with even small amounts of material a date can be determined (e.g., when dating a pottery shard or a target mineral of low natural abundance). The caveat is that any sensitivity changes which occur during a measurement sequence must be accounted for. In optical dating, this is achieved by monitoring the response to some uniform ‘test dose,’ administered during every measurement cycle. For TL measurements, however, the initial

25 heating measurement can alter the shape of subsequent regenerative glow curves, rendering this ap-  
26 proach of ‘stripping out’ sensitivity change by monitoring test dose responses as inadequate, because  
27 only certain regions within the curve will become more or less sensitive to irradiation (in some cases,  
28 this is overcome by monitoring the changes in peak heights through measurement cycles, although  
29 this incorporates further assumptions; [Adamiec et al., 2006](#)). In the case of such TL shape changes  
30 upon heating, the MAAD approach is ideal for constructing dose-response curves, as all of the dose  
31 responses should exhibit natural luminescence efficiency (an exception would be a radiation-induced  
32 change in sensitivity; [Zimmerman, 1971](#)).

## 33 **2. Samples and instrumentation**

34 The K-feldspar samples analyzed in this study were extracted from bedrock outcrops across the  
35 southern San Bernardino Mountains of Southern California. Young apatite (U-Th)/He ages ([Spotila  
36 et al., 1998, 2001](#)) and catchment-averaged cosmogenic  $^{10}\text{Be}$  denudation rates from this region  
37 ([Binnie et al., 2007, 2010](#)) reveal a landscape which is rapidly eroding in response to transpressional  
38 uplift across the San Andreas fault system. Accordingly, we expect the majority of these samples to  
39 have cooled rapidly during the latest Pleistocene, maintaining natural trap occupancy below field  
40 saturation which is a requirement for luminescence thermochronometry ([King et al., 2016a](#)).

41 Twelve bedrock samples were removed from outcrops using a chisel and hammer. After collec-  
42 tion, samples were spray-painted with a contrasting color and then broken into smaller pieces under  
43 dim amber LED lighting. The sunlight-exposed, outer-surface portions of the bedrock samples were  
44 separated from the inner portions. The unexposed inner portions of rock were then gently ground  
45 with a pestle and mortar and sieved to isolate the 175 - 400  $\mu\text{m}$  size fraction. These separates were  
46 treated with 3% hydrochloric acid and separated by density using lithium metatungstate heavy  
47 liquid ( $\rho < 2.565 \text{ g/cm}^3$ ; [Rhodes 2015](#)) in order to isolate the most potassic feldspar grains. Under

48 a binocular scope, three K-feldspar grains were manually placed into the center of each stainless  
49 steel disc for luminescence measurements.

50 All luminescence measurements were performed at the UCLA luminescence laboratory using a  
51 TL-DA-20 Risø automated reader equipped with a  $^{90}\text{Sr}/^{90}\text{Y}$  beta source which delivers 0.1 Gy/s  
52 at the sample location (Bøtter-Jensen et al., 2003). Emissions were detected through a Schott  
53 BG3-BG39 filter combination (transmitting between  $\sim 325 - 475$  nm). Thermoluminescence mea-  
54 surements were performed in a nitrogen atmosphere and glow curves were measured at a heating  
55 rate of 0.5 °C/s to avoid thermal lag between the disc and the mounted grains.

### 56 3. Measurements

57 To characterize the dose-response characteristics of each sample, 15 aliquots were measured for  
58 each of the 12 bedrock samples. Additive doses were: 0 ( $n = 6$ ; natural dose only), 50 ( $n = 1$ ), 100  
59 ( $n = 1$ ), 500 ( $n = 1$ ), 1000 ( $n = 3$ ), and 5000 Gy ( $n = 3$ ). The measurement sequence for each disc  
60 is shown in Table 1. Discs were heated from 0 to 500 °C at a rate of 0.5 °C/s, with TL intensity  
61 recorded at 1 °C increments (Fig. S1).

62 Thermoluminescence signals following laboratory irradiation (regenerative TL) of K-feldspar  
63 samples are known to fade on laboratory timescales (Wintle, 1973; Riedesel et al., 2021). To  
64 quantify this effect in our samples, we prepared 10 natural aliquots per sample. These aliquots  
65 were first preheated to 100 °C for 10 s at a rate of 10 °C/s and then heated to 310 °C at a rate of  
66 0.5 °C/s. The first heat treatment is identical to the preheat used in the dose response experiment  
67 described in the previous section. The second heat is analogous to the subsequent TL glow curve  
68 readout (step 3 in Table 1), but the peak temperature of 310 °C is significantly lower than the peak  
69 temperature used in the MAAD dose response experiment. This lower peak temperature was chosen  
70 to be just higher than the region of interest within the TL glow curve (150-300 °C), to minimize

71 changes in TL recombination kinetics induced by heating, and ultimately, to evict the natural TL  
 72 charge population within this measurement temperature bin.

73 Following these initial heatings, aliquots were given a beta dose of 50 Gy, preheated to 100 °C  
 74 for 10 s at a rate of 10 °C/s and then held at room temperature for a set time (Auclair et al., 2003).  
 75 Per sample, two aliquots each were stored for times of approximately 3 ks, 10 ks, 2 d, 1 wk and  
 76 3 wk. Following storage, aliquots were measured following steps 3 - 8 of Table 1. Typical fading  
 77 behavior is shown for sample J1499 in Fig. 2 and for all samples in Fig. S2.

#### 78 4. Extracting kinetic parameters from measurements

79 To extract kinetic parameters from our measurements, we use the localized transition model of  
 80 Brown et al. (2017), which assumes first-order trapping and TL emission by excited-state tunneling  
 81 to the nearest radiative recombination center (Huntley, 2006; Jain et al., 2012; Pagonis et al., 2016).  
 82 This model is physically plausible, relies on minimal free parameters, and successfully captures  
 83 the observed dependence of natural TL (NTL)  $T_{1/2}$  (measurement temperature at half-maximum  
 84 intensity for the bulk TL glow curve) on geologic burial temperatures and laboratory preheating  
 85 experiments (Brown et al., 2017; Pagonis and Brown, 2019). Additionally, the model explains the  
 86 more subtle decrease in NTL  $T_{1/2}$  values with greater geologic dose rates (Brown and Rhodes, 2019)  
 87 and the lack of regenerative TL (RTL)  $T_{1/2}$  variation following a range of laboratory doses (Pagonis  
 88 et al., 2019).

89 The kinetic model is expressed as:

$$90 \quad \frac{dn(r')}{dt} = \frac{\dot{D}}{D_0} \left( N(r') - n(r') \right) - n(r') \exp \left( - \Delta E / k_B T \right) \frac{P(r')s}{P(r') + s} \quad (1)$$

92 where  $n(r')$  and  $N(r')$  are the concentrations ( $\text{m}^{-3}$ ) of occupied and total trapping sites, respec-  
 93 tively, at a dimensionless recombination distance  $r'$ ;  $\dot{D}$  is the geologic dose rate (Gy/ka);  $D_0$  is the  
 94 characteristic dose of saturation (Gy);  $\Delta E$  is the activation energy difference between the ground-

95 and excited-states (eV);  $T$  is the absolute temperature of the sample (K);  $k_B$  is the Boltzmann con-  
96 stant (eV/K);  $P(r')$  is the tunneling probability at some distance  $r'$  ( $\text{s}^{-1}$ ); and  $s$  is the frequency  
97 factor ( $\text{s}^{-1}$ ).

## 98 5. Kinetic parameters

99 We compared results from Eq. 1 with the fading and dose response datasets to estimate the  
100 recombination center density  $\rho$  ( $\text{m}^{-3}$ ) and the activation energy  $\Delta E$  of each sample using a Monte  
101 Carlo approach. First, we compared the  $T_{1/2}$  values from room temperature fading measurements  
102 (Fig. 2) with modeled values produced using Eq. 1 (Fig. 2). For each of the 5000 iterations, values of  
103  $\rho$  and  $\Delta E$  were randomly selected within the ranges of  $10^{24} - 10^{28} \text{ m}^{-3}$  and 0.8 - 1.2 eV, respectively.  
104 As illustrated in Fig. 2, higher  $\Delta E$  values produce less time dependence of  $T_{1/2}$  decay and higher  
105  $\rho$  values reduce  $T_{1/2}$  values at all delay times. Data misfit was quantified with the error weighted  
106 sum of squares for all fade durations and the best-fit fifth and tenth percentile contours for these  
107 simulations are shown in blue in Fig. 4.

108 Next, we compared the shape of the MAAD TL curves following the 5 kGy additive dose  
109 with that predicted by Eq. 1. Specifically, on a semilog plot of TL intensity versus measurement  
110 temperature, the slope of the high-temperature limb of the TL glow curve (defined here as 220 -  
111 300 °C) steepens significantly at greater  $\rho$  values, whereas variations in  $\Delta E$  values produce only  
112 slight differences (Fig. 3). Using the same approach and parameter ranges as above, we plot the  
113 best-fit fifth and tenth percentile contours in red in Fig. 4. Significantly, the best-fit contours for  $\rho$   
114 and  $\Delta E$  overlap when the fading and curve shape datasets are combined. Values consistent with  
115 both the tenth percentile contours of each sample are listed in Table 2.

116 Notice that we evaluate the dimensional  $\rho$  rather than the commonly used dimensionless  $\rho'$   
117 to disentangle  $\rho$  and  $\Delta E$ . Within the localized transition model,  $\rho'$  embeds depth of the excited

118 state within the tunneling probability term (e.g., Eq. 2 of [Jain et al., 2012](#)). Assuming a fixed  
119 ground-state energy level ([Brown and Rhodes, 2017](#)), variation in  $\rho'$  then also implies variation in  
120  $\Delta E$ . Therefore, we isolate these two parameters during data misfit analysis, though we ultimately  
121 translate the best-fit  $\rho$  into  $\rho'$  using the independently optimized  $\Delta E$  value.

122  $D_0$  values were estimated by comparing measured and simulated TL dose response intensities.  
123 Simulated growth curves were produced with Eq. 1, using the best-fit  $\rho$  and  $\Delta E$  values listed  
124 in Table 2. We assume that frequency factors  $P_0$  and  $s$  equal  $3 \times 10^{15} \text{ s}^{-1}$  ([Huntley, 2006](#)) and  
125 the ground-state depth  $E_g$  is 2.1 eV ([Brown and Rhodes, 2017](#)). Results from 1000 Monte Carlo  
126 iterations for sample J1500 are shown in Fig. 5, with the mean and standard deviation of the best-fit  
127 fifth percentile values plotted as a red diamond.

## 128 6. Fractional saturation values

129 Figure 6 shows the ratio of the natural TL signals to the ‘natural + 5 kGy’ TL signals. Each  
130 ratio shown in Fig. 6 represents the mean and standard deviation of ratios from 6 natural and 3  
131 ‘natural + 5kGy’ aliquots (18 ratios per sample per channel). 10 of 108 aliquots were excluded  
132 based on irregular glow curve shapes.

133 The additive dose responses were corrected for fading during laboratory irradiation, prior to  
134 measurement using the kinetic parameters in Table 2 and the approach of [Kars et al. \(2008\)](#),  
135 modified for the localized transition model (e.g., Eq. 14 of [Jain et al., 2015](#)). Assuming that an  
136 additive dose of 5 kGy will fully saturate the source luminescence traps (a reasonable assumption  
137 based on the  $D_0$  values in Table 2), these  $N/(N + 5 \text{ kGy})$  ratios are assumed to represent the  
138 fractional saturation values for each measurement temperature channel at laboratory dose rates,  
139  $\frac{n}{N}(T)$ , where  $T = 150 - 300 \text{ }^\circ\text{C}$  with step sizes of  $1 \text{ }^\circ\text{C}$ . That  $\frac{n}{N}(T)$  values of all samples fall within  
140 the range of 0 to 1 at  $1\sigma$  supports this assumption.

141 Likewise, the differences in  $N/(N + 5 \text{ kGy})$  ratios between samples shown in Fig. 6 are expected  
142 from their position within the landscape. Sample J0172 ( $N/(N + 5 \text{ kGy}) \lesssim 0.2$ ) is taken from the  
143 base of a rocky cliff with abundant evidence of modern rockfall. Sample J0216 ( $N/(N + 5 \text{ kGy}) \lesssim$   
144 0.4) is taken from a hillside near the base of the mountains and sample J1502 ( $N/(N + 5 \text{ kGy}) \lesssim$   
145 1.0) is taken from a soil-mantled spur. In other words, geomorphic evidence suggests that recent  
146 exhumation rates are greatest for sample J0172, less for J0216, and least for J1502. As cooling rate  
147 is assumed to scale with exhumation rate, it is encouraging that the calculated  $N/(N + 5 \text{ kGy})$   
148 ratios for these samples follow this pattern.

## 149 7. Conclusions

150 The kinetic parameters (Table 2) determined using the approach described here and summarized  
151 in Fig. 1 are consistent with previous estimates for K-feldspar TL signals in the low-temperature  
152 region of the glow curve that assume excited-state tunneling as the primary recombination pathway  
153 (Sfampa et al., 2015; Brown et al., 2017; Brown and Rhodes, 2019) as well as numerical results  
154 from localized transition models (Jain et al., 2012; Pagonis et al., 2021). Additionally, the  $\rho$  and  
155  $\Delta E$  values determined by data-model misfit of  $T_{1/2}$  fading measurements (Fig. 2) and by of glow  
156 curve shape measurements (Fig. 3) yield mutually consistent results. By combining these analyses,  
157 the best-fit region is considerably reduced, giving more precise estimates of both  $\rho$  and  $\Delta E$  (Fig. 4)  
158 which can then be incorporated into the determination of  $D_0$  (Fig. 5). This approach has potential  
159 to produce reliable kinetic parameters to better understand the time-temperature history of bedrock  
160 K-feldspar samples.

## 161 Acknowledgements

162 We thank Tomas Capaldi, Andreas Lang, Natalia Solomatova and David Sammeth for help with  
163 sample collection. Brown acknowledges funding by National Science Foundation award number

164 1806629.

165 **References**

- 166 Adamiec, G., Bluszcz, A., Bailey, R., Garcia-Talavera, M., 2006. Finding model parameters: Genetic  
167 algorithms and the numerical modelling of quartz luminescence. *Radiation Measurements* 41,  
168 897–902.
- 169 Auclair, M., Lamothe, M., Huot, S., 2003. Measurement of anomalous fading for feldspar IRSL  
170 using SAR. *Radiation Measurements* 37, 487–492.
- 171 Binnie, S.A., Phillips, W.M., Summerfield, M.A., Fifield, L.K., 2007. Tectonic uplift, threshold  
172 hillslopes, and denudation rates in a developing mountain range. *Geology* 35, 743–746.
- 173 Binnie, S.A., Phillips, W.M., Summerfield, M.A., Fifield, L.K., Spotila, J.A., 2010. Tectonic and cli-  
174 matic controls of denudation rates in active orogens: The San Bernardino Mountains, California.  
175 *Geomorphology* 118, 249–261.
- 176 Biswas, R.H., Herman, F., King, G.E., Braun, J., 2018. Thermoluminescence of feldspar as a multi-  
177 thermochronometer to constrain the temporal variation of rock exhumation in the recent past.  
178 *Earth and Planetary Science Letters* 495, 56–68.
- 179 Biswas, R.H., Herman, F., King, G.E., Lehmann, B., Singhvi, A.K., 2020. Surface paleothermometry  
180 using low-temperature thermoluminescence of feldspar. *Climate of the Past* 16, 2075–2093.
- 181 Bøtter-Jensen, L., Andersen, C.E., Duller, G.A.T., Murray, A.S., 2003. Developments in radiation,  
182 stimulation and observation facilities in luminescence measurements. *Radiation Measurements*  
183 37, 535–541.
- 184 Brown, N.D., Rhodes, E.J., 2017. Thermoluminescence measurements of trap depth in alkali  
185 feldspars extracted from bedrock samples. *Radiation Measurements* 96, 53–61.

186 Brown, N.D., Rhodes, E.J., 2019. Dose-rate dependence of natural tl signals from feldspars extracted  
187 from bedrock samples. *Radiation Measurements* 128, 106188.

188 Brown, N.D., Rhodes, E.J., Harrison, T.M., 2017. Using thermoluminescence signals from feldspars  
189 for low-temperature thermochronology. *Quaternary Geochronology* 42, 31–41.

190 Guralnik, B., Jain, M., Herman, F., Ankjaergaard, C., Murray, A.S., Valla, P.G., Preusser, F.,  
191 King, G.E., Chen, R., Lowick, S.E., Kook, M., Rhodes, E.J., 2015. OSL-thermochronometry of  
192 feldspar from the KTB borehole, Germany. *Earth and Planetary Science Letters* 423, 232 – 243.

193 Herman, F., Rhodes, E.J., Braun, J., Heiniger, L., 2010. Uniform erosion rates and relief am-  
194 plitude during glacial cycles in the Southern Alps of New Zealand, as revealed from OSL-  
195 thermochronology. *Earth and Planetary Science Letters* 297, 183–189.

196 Huntley, D.J., 2006. An explanation of the power-law decay of luminescence. *Journal of Physics:*  
197 *Condensed Matter* 18, 1359–1365.

198 Jain, M., Guralnik, B., Andersen, M.T., 2012. Stimulated luminescence emission from localized  
199 recombination in randomly distributed defects. *Journal of Physics: Condensed Matter* 24, 385402.

200 Jain, M., Sohpati, R., Guralnik, B., Murray, A.S., Kook, M., Lapp, T., Prasad, A.K., Thomsen,  
201 K.J., Buylaert, J.P., 2015. Kinetics of infrared stimulated luminescence from feldspars. *Radiation*  
202 *Measurements* 81, 242–250.

203 Kars, R., Wallinga, J., Cohen, K., 2008. A new approach towards anomalous fading correction for  
204 feldspar IRSL dating–tests on samples in field saturation. *Radiation Measurements* 43, 786–790.

205 King, G.E., Guralnik, B., Valla, P.G., Herman, F., 2016a. Trapped-charge thermochronometry and  
206 thermometry: A status review. *Chemical Geology* 446, 3–17.

207 King, G.E., Herman, F., Lambert, R., Valla, P.G., Guralnik, B., 2016b. Multi-OSL-  
208 thermochronometry of feldspar. *Quaternary Geochronology* 33, 76–87.

209 Li, B., Li, S.H., 2012. Determining the cooling age using luminescence-thermochronology. *Tectono-*  
210 *physics* 580, 242–248.

211 Pagonis, V., Ankjaergaard, C., Jain, M., Chithambo, M.L., 2016. Quantitative analysis of time-  
212 resolved infrared stimulated luminescence in feldspars. *Physica B: Condensed Matter* 497, 78–85.

213 Pagonis, V., Brown, N.D., 2019. On the unchanging shape of thermoluminescence peaks in pre-  
214 heated feldspars: Implications for temperature sensing and thermochronometry. *Radiation Mea-*  
215 *surements* 124, 19–28.

216 Pagonis, V., Brown, N.D., Peng, J., Kitis, G., Polymeris, G.S., 2021. On the deconvolution of  
217 promptly measured luminescence signals in feldspars. *Journal of Luminescence* 239, 118334.

218 Pagonis, V., Brown, N.D., Polymeris, G.S., Kitis, G., 2019. Comprehensive analysis of thermolu-  
219 minescence signals in  $\text{mgB}_4\text{O}_7:\text{Dy,Na}$  dosimeter. *Journal of Luminescence* 213, 334–342.

220 Rhodes, E.J., 2015. Dating sediments using potassium feldspar single-grain IRSL: initial method-  
221 ological considerations. *Quaternary International* 362, 14–22.

222 Riedesel, S., Bell, A.M.T., Duller, G.A.T., Finch, A.A., Jain, M., King, G.E., Pearce, N.J., Roberts,  
223 H.M., 2021. Exploring sources of variation in thermoluminescence emissions and anomalous fading  
224 in alkali feldspars. *Radiation Measurements* 141, 106541.

225 Sfampa, I., Polymeris, G., Pagonis, V., Theodosoglou, E., Tsirliganis, N., Kitis, G., 2015. Correlat-  
226 ion of basic TL, OSL and IRSL properties of ten K-feldspar samples of various origins. *Nuclear*  
227 *Instruments and Methods in Physics Research B* 359, 89–98.

228 Spotila, J., Farley, K., Sieh, K., 1998. Uplift and erosion of the San Bernardino Mountains associated  
229 with transpression along the San Andreas fault, California, as constrained by radiogenic helium  
230 thermochronometry. *Tectonics* 17, 360–378.

231 Spotila, J., Farley, K., Yule, J., Reiners, P., 2001. Near-field transpressive deformation along the  
232 San Andreas fault zone in southern California, based on exhumation constrained by (U-Th)/He  
233 dating. *Journal of Geophysical Research* 106, 30909–30922.

234 Wintle, A., 1973. Anomalous fading of thermoluminescence in mineral samples. *Nature* 245, 143–  
235 144.

236 Wintle, A., Murray, A., 2006. A review of quartz optically stimulated luminescence characteristics  
237 and their relevance in single-aliquot regeneration dating protocols. *Radiation Measurements* 41,  
238 369–391.

239 Zimmerman, J., 1971. The radiation-induced increase of the 100C thermoluminescence sensitivity  
240 of fired quartz. *Journal of Physics C: Solid State Physics* 4, 3265–3276.

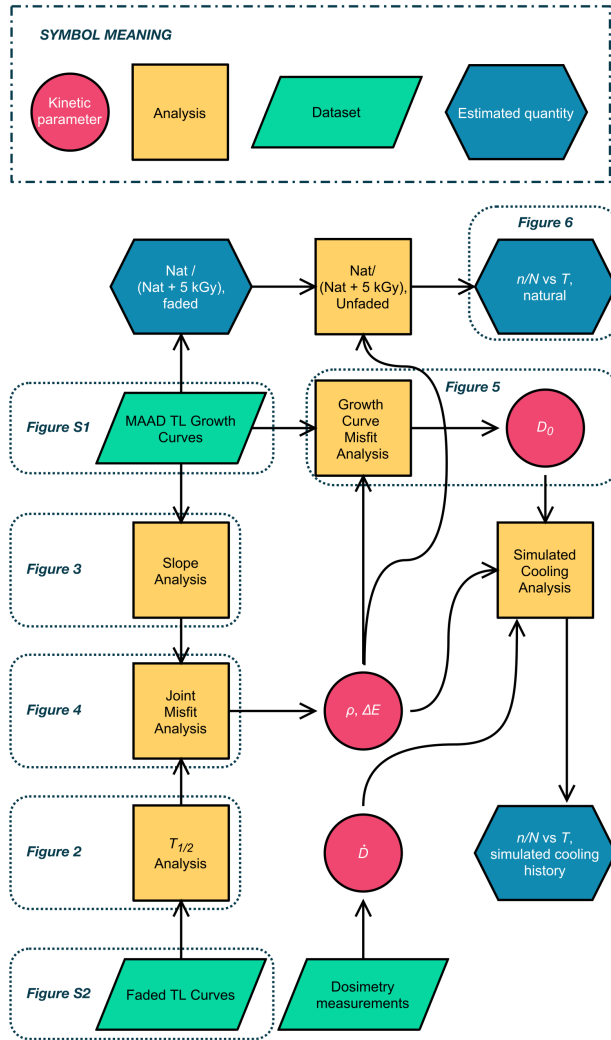


Figure 1: Flowchart illustrating how datasets (green parallelograms) are analyzed (yellow squares) to derive luminescence kinetic parameters (red circles) and other quantities (blue hexagons) to ultimately arrive at fractional saturation as a function of measurement temperature. Figures corresponding to various steps are cross-referenced.

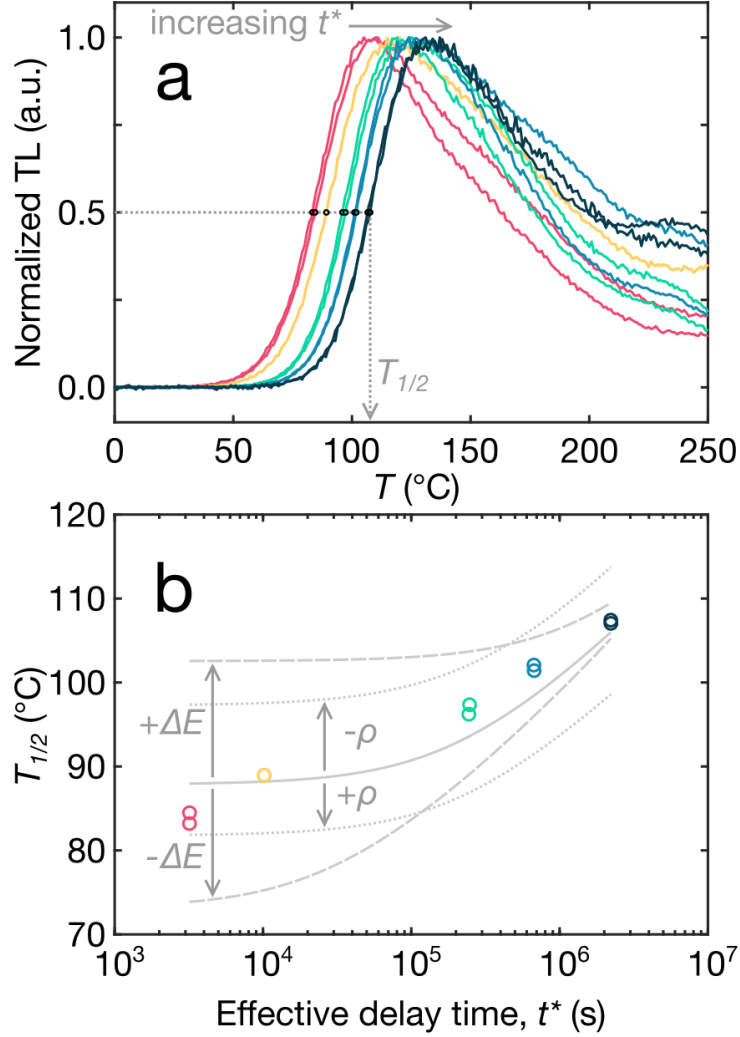


Figure 2: (a) Normalized TL curves of sample J1499 are shown following effective delay times ( $t^*$ ) ranging from 3197 s (red curves) to 25.7 d (dark blue curves). (b)  $T_{1/2}$  values from these glow curves are plotted as a function of  $t^*$  (circles). Several simulated datasets are shown for comparison to illustrate the effects of varying luminescence parameters  $\Delta E$  (values of 1.10, 1.15, and 1.20 eV shown) and  $\rho$  ( $10^{26.5}$ ,  $10^{27.0}$ , and  $10^{27.5}$   $\text{m}^{-3}$  shown).

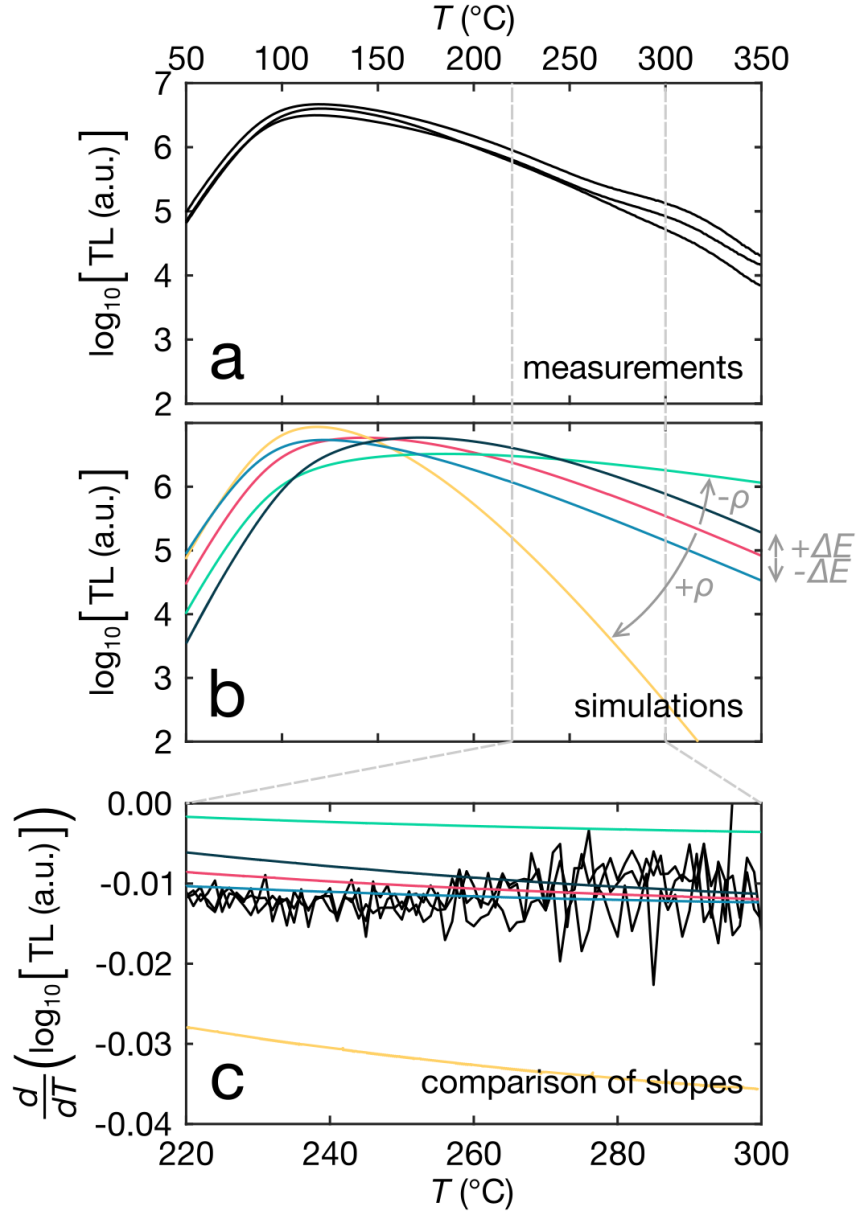


Figure 3: (a) Sensitivity-corrected TL curves for three aliquots of sample J0165 following an additive dose of 5 kGy. The  $y$ -axis scaling is logarithmic. (b) Five MAAD TL curves are plotted for comparison to illustrate the effects of varying luminescence parameters  $\Delta E$  (values of 1.0, 1.1, and 1.2 eV shown) and  $\rho$  ( $10^{25.65}$ ,  $10^{26.15}$ , and  $10^{26.65} \text{ m}^{-3}$  shown). (c) The first derivatives of both datasets are plotted together. Note the sensitivity of model fit to  $\rho$  value.

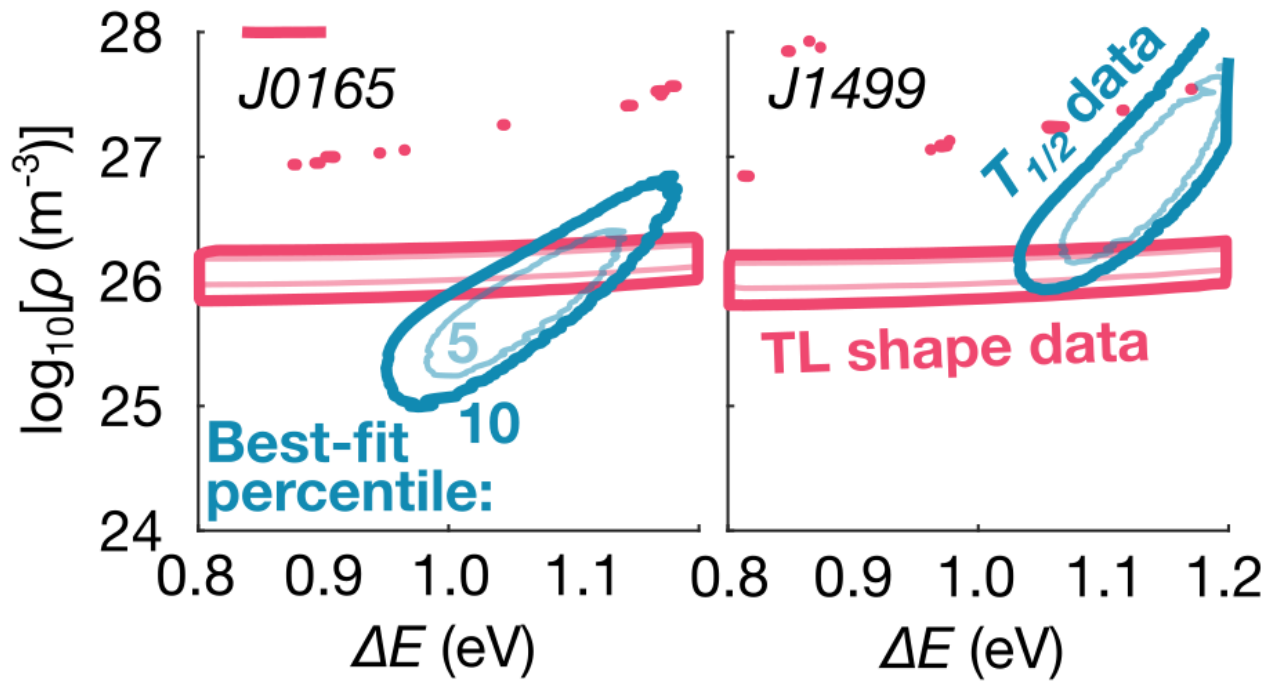


Figure 4: Contours are shown for the 5<sup>th</sup> and 10<sup>th</sup> best-fit percentiles of Monte Carlo simulations reproducing TL glow curve shape (red contours) and  $T_{1/2}$  dependence on laboratory storage time (blue contours) based upon randomly selected values for parameters  $\rho$  and  $\Delta E$ .

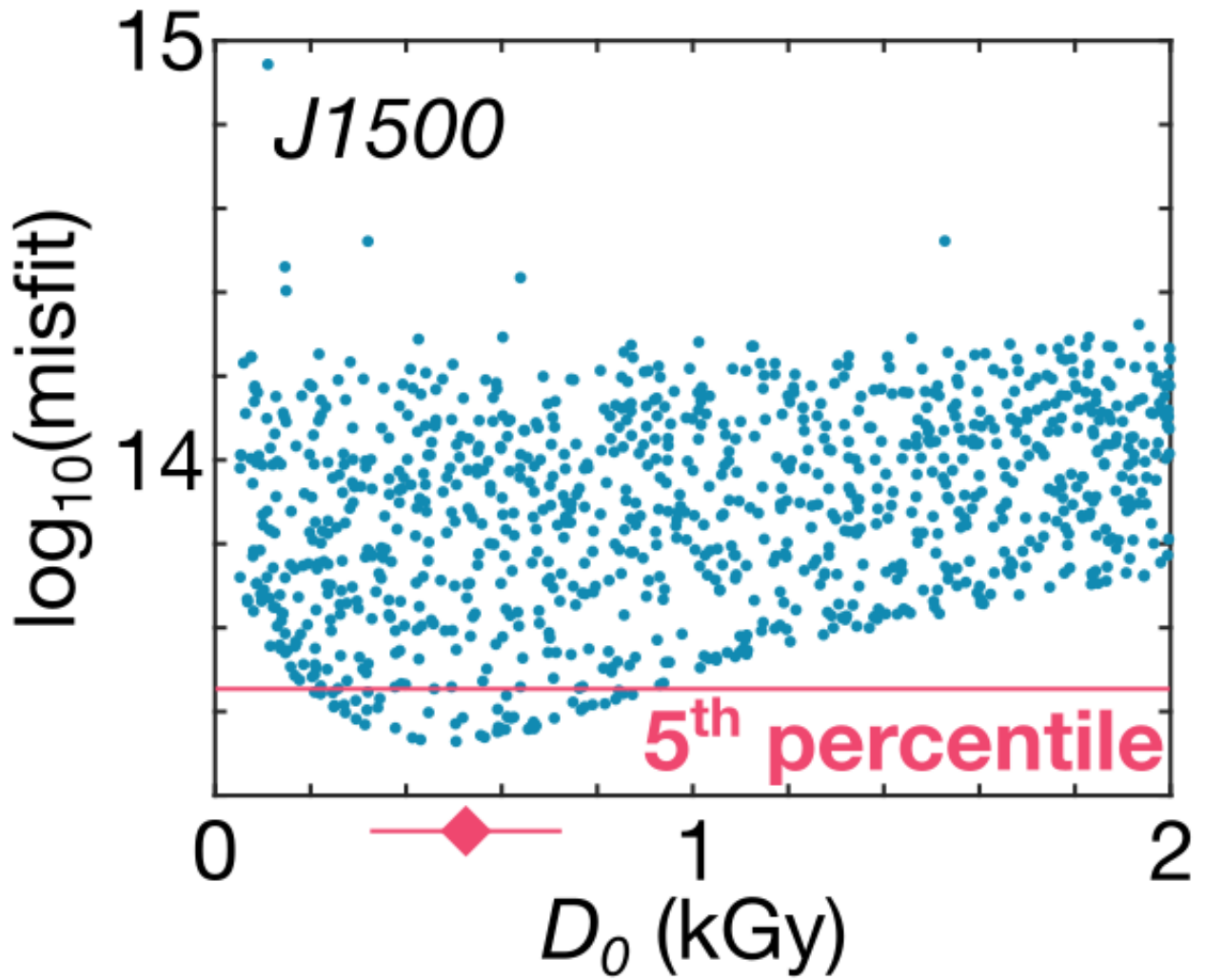


Figure 5: Calculated misfit between measured and simulated TL dose response data as a function of chosen  $D_0$  value, using optimized  $\rho'$  and  $\Delta E$  values listed in Table 2. Monte Carlo iterations from the best-fit 5<sup>th</sup> percentile are used to calculate the  $D_0$ , represented by the diamond with error bars and also listed in Table 2.

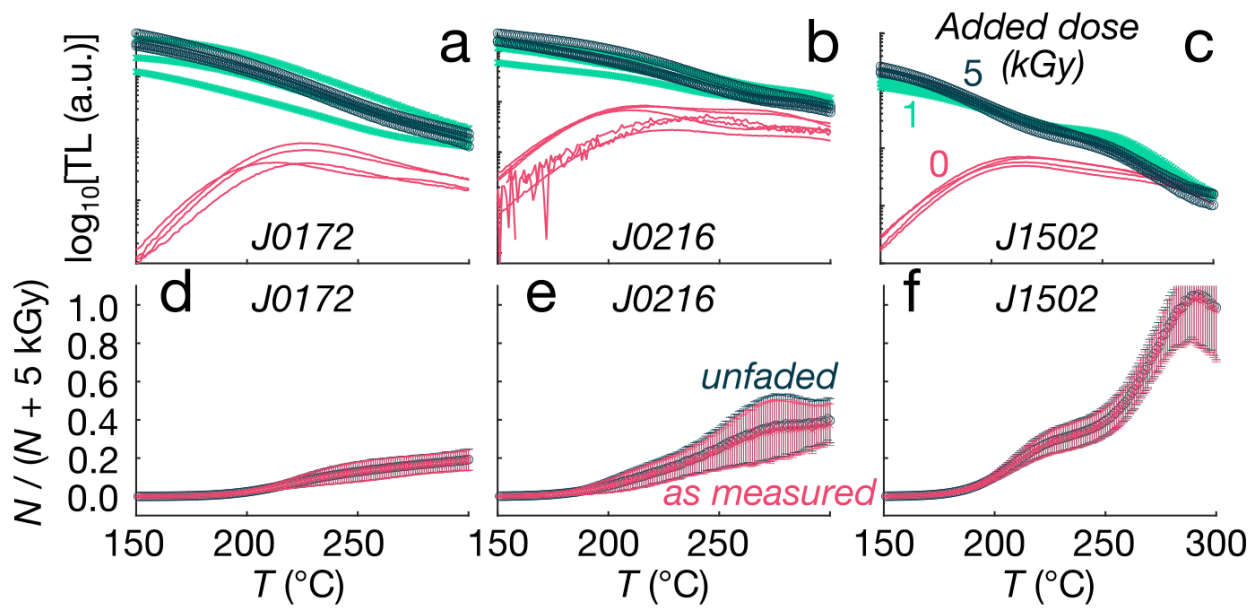


Figure 6: (a - c) The sensitivity-corrected natural (red curves), ‘natural + 1 kGy’ (green Xs), and ‘natural + 5 kGy’ (dark blue circles) TL glow curves are shown for samples J0172, J0216, and J1502, with a logarithmic  $y$ -axis. Each glow curve is a separate aliquot. (d - f) The ‘natural / (natural + 5 kGy)’ data are plotted as measured (red Xs) and unfaded (blue circles).

Table 1: Thermoluminescence measurement sequence.

Step	Treatment	Purpose
1	Additive dose, $D = 0 - 5000$ Gy	Populate luminescence traps
2	Preheat ( $T = 100$ °C, 10 s)	Remove unstable signal
3	TL (0.5 °C/s)	Luminescence intensity, $L$
4	TL (0.5 °C/s)	Background intensity
5	Test dose, $D_t = 10$ Gy	Constant dose for normalization
6	Preheat ( $T = 100$ °C, 10 s)	Remove unstable signal
7	TL (0.5 °C/s)	Test dose intensity, $T$
8	TL (0.5 °C/s)	Background intensity

Table 2: Thermoluminescence kinetic parameters.

Sample	$D_0$ (Gy)	$\Delta E$ (eV)	$\rho' \times 10^{-4}$
J0165	$1664 \pm 194$	$1.08 \pm 0.08$	$7.10 \pm 3.94$
J0172	$1411 \pm 318$	$1.10 \pm 0.06$	$7.65 \pm 3.65$
J0214	$1008 \pm 300$	$1.08 \pm 0.08$	$6.47 \pm 3.59$
J0216	$1097 \pm 418$	$1.04 \pm 0.09$	$5.08 \pm 2.69$
J0218	$936 \pm 463$	$1.04 \pm 0.07$	$5.08 \pm 2.42$
J1298	$1282 \pm 328$	$1.10 \pm 0.06$	$10.57 \pm 5.58$
J1299	$1175 \pm 362$	$1.11 \pm 0.07$	$10.48 \pm 5.54$
J1300	$1006 \pm 438$	$1.09 \pm 0.06$	$7.54 \pm 4.18$
J1499	$932 \pm 507$	$1.08 \pm 0.05$	$6.78 \pm 3.23$
J1500	$527 \pm 200$	$1.09 \pm 0.06$	$7.54 \pm 3.99$
J1501	$959 \pm 326$	$1.11 \pm 0.06$	$10.73 \pm 5.67$
J1502	$1287 \pm 325$	$1.10 \pm 0.06$	$11.32 \pm 5.69$

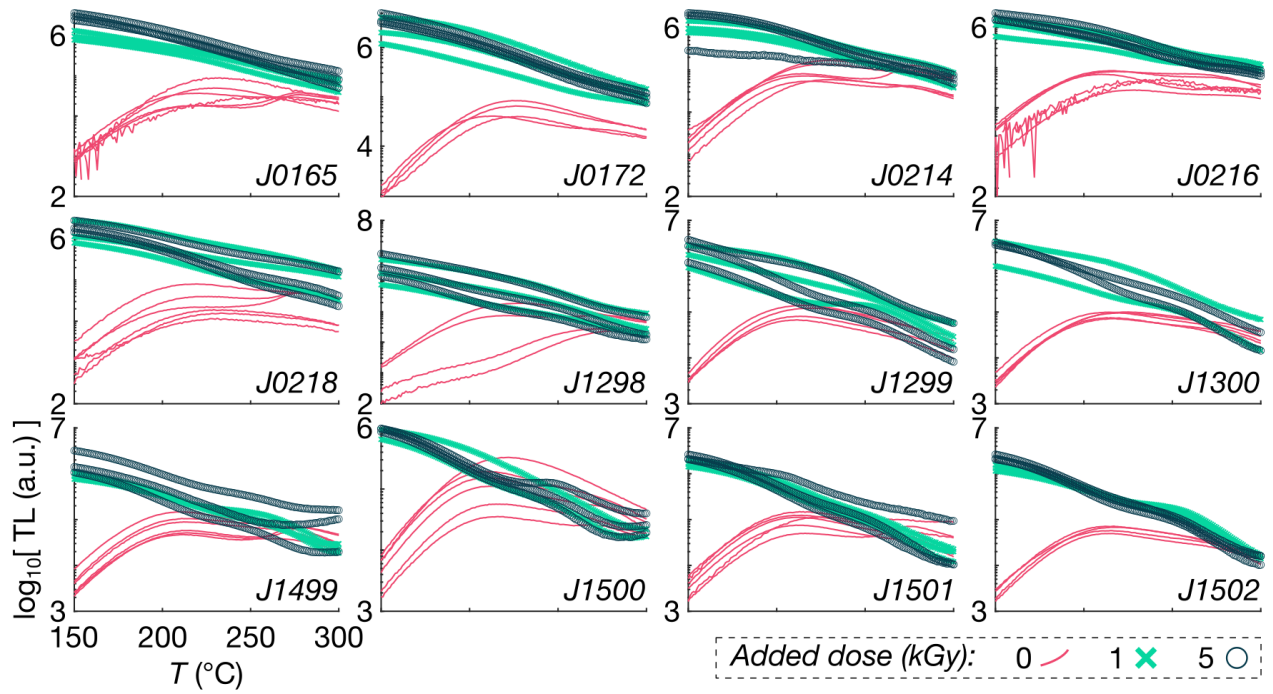


Figure S1: The sensitivity-corrected natural (red curves), ‘natural + 1 kGy’ (green Xs), and ‘natural + 5 kGy’ (dark blue circles) TL glow curves are shown for all samples, with a logarithmic  $y$ -axis. Each glow curve is a separate aliquot.

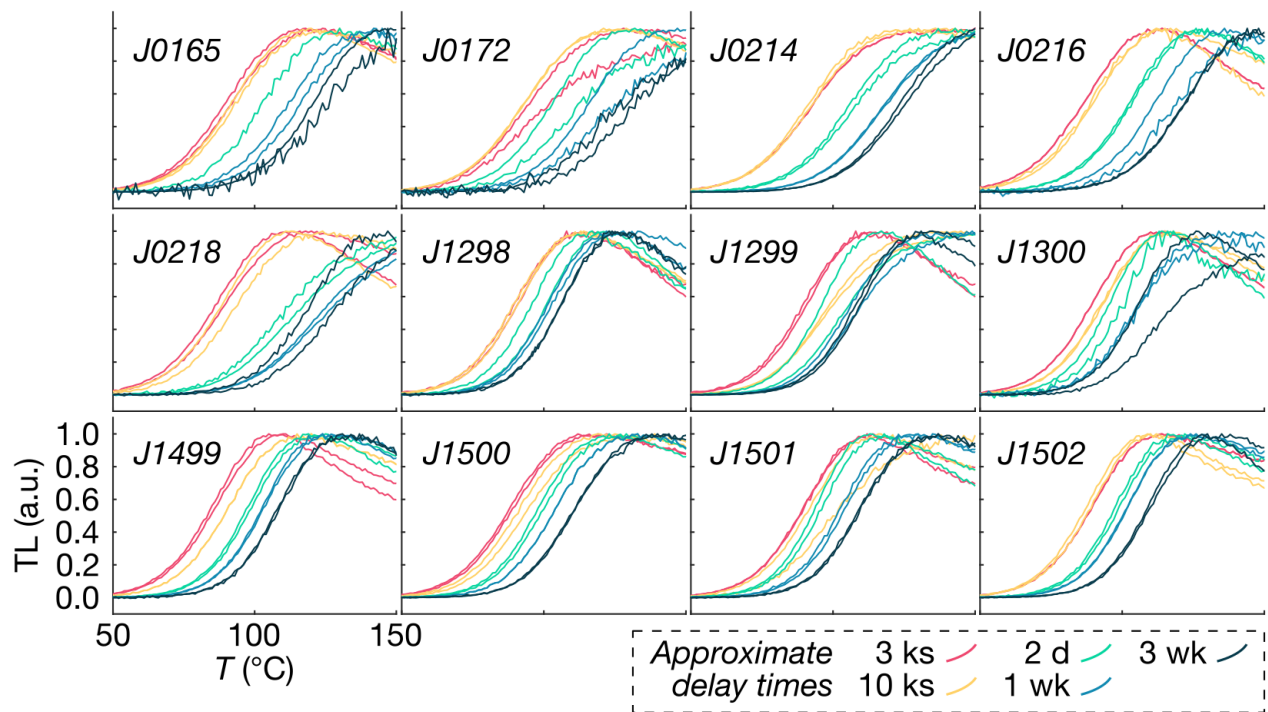


Figure S2: Intensity normalized TL glow curves following a laboratory dose of 50 Gy followed by a preheat and then various room temperature storage durations, ranging from about 3 ks to 3 wk. Each delay time is represented by two aliquots per sample.